Bulletin of Mathematical Biology (2007)
DOI 10.1007/s11538-006-9180-y

ORIGINAL ARTICLE

Emergent Features Due to Grid-Cell Biology: Synchronisation in Biophysical Models

E. J. Guirey[a,b,*], M. A. Bees[b], A. P. Martin[a], M. A. Srokosz[a], M. J. R. Fasham[a]

[a] *National Oceanography Centre Southampton, European Way, Southampton SO14 3ZH, UK*
[b] *Department of Mathematics, University of Glasgow, University Gardens, Glasgow G12 8QW, UK*

Received: 25 April 2006 / Accepted: 2 November 2006

Abstract Modelling studies of upper ocean phenomena, such as that of the spatial and temporal patchiness in plankton distributions, typically employ coupled biophysical models, with biology in each grid-cell represented by a plankton ecosystem model. It has not generally been considered what impact the choice of grid-cell ecosystem model, from the many developed in the literature, might have upon the results of such a study. We use the methods of synchronisation theory, which is concerned with ensembles of interacting oscillators, to address this question, considering the simplest possible case of a chain of identically represented interacting plankton grid-cells. It is shown that the ability of the system to exhibit stably homogeneous (fully synchronised) dynamics depends crucially upon the choice of biological model and number of grid-cells, with dynamics changing dramatically at a threshold strength of mixing between grid-cells. Consequently, for modelling studies of the ocean the resolution chosen, and therefore number of grid-cells used, could drastically alter the emergent features of the model. It is shown that chaotic ecosystem dynamics, in particular, should be used with care.

Keywords Plankton patchiness · Synchronisation · Metapopulation · Biophysical modelling

1. Introduction

The growing awareness of possible anthrogenic forcing of the global carbon cycle has increased interest in its study. Since phytoplanktons are the primary producers of the marine ecosystem (Lalli and Parsons, 1997), a study of the global car-

*Corresponding author.
E-mail address: ejg@noc.soton.ac.uk (E. J. Guirey).

bon cycle is impossible without a model of the upper ocean ecosystem (Popova, 1995). Such models attempt to break down the complicated structure of a marine ecosystem into a number of components and the flows between them. A wide range of models exists, reflecting the variety of ocean regions and modelling aims that have been the concerns of different studies (Totterdell, 1993). In standard carbon cycle studies, such an ecosystem model is usually assumed to have geographical generality and is embedded in a general ocean circulation model (e.g., Slater, 1993). The resulting biophysical model of the carbon cycle can then be examined for its ability to predict features of phytoplankton distribution and production observed in the real ocean.

One such feature, observed from ships (see Bainbridge, 1956) as discoloured patches of water, in collected biological data (e.g., Popova et al., 2002) and, more recently, in satellite imagery, is the heterogeneous (or patchy) nature of plankton distributions in space and time. Despite much recent progress, this "patchiness" and its consequences are not fully understood (Martin, 2003) and it is a phenomenon worthy of study not least because of an evident link with levels of primary production (Smith et al., 1996; Martin and Richards, 2002). Plankton distributions are patchy on length-scales of centimetres to several hundred kilometres, raising the question of what sets the spatial scales of structure observed. Modelling studies may attempt to use the output from coupled biophysical models to answer such questions (e.g., Abraham, 1998; Levy and Klein, 2004).

In essence, the usual biophysical model consists of an ensemble of interacting grid-cells, in each of which the biology evolves according to the chosen ecosystem model, with the interaction provided by the prescribed physical circulation model. Such a system becomes the concern of the area of mathematics known as synchronisation theory, which studies how the natural rhythms of individually oscillating objects adjust as a result of couplings between them (Pikovsky et al., 2001). If the coupling causes the oscillations to become identical in time, then we describe the system as synchronised.

The earliest recorded interest in a phenomenon of this kind was by Christiaan Huygens, the Dutch Astronomer, Mathematician and Physicist, who observed in 1673 how two swinging pendulum clocks hanging from a wooden beam may become phase-locked as a result of vibrations, caused by the motion, travelling along the beam (Pikovsky et al., 2001).

More recently, synchrony has also been observed in the dynamics of natural populations. One study, by Grenfall et al. (1998), looked at fluctuations in the density of feral sheep populations on separate islands. Fluctuations exhibited a high degree of synchrony, despite no direct link existing between the populations. In this case, the synchronising influence was understood to be the indirect correlating effect of a common environmental forcing. Another well-studied example is the cycle of Canadian lynx numbers (Elton and Nicholson, 1942), which oscillate on a roughly 10-year cycle. Remarkably, the abundances in regions thousands of miles apart are in phase, although amplitudes differ. This phase-synchronisation has been shown by Blasius and Stone (2000), who considered the lynx distribution as a lattice of coupled oscillating "patches," to be at least partly due to migration of animals between adjacent regions.

Hillary and Bees (2004) studied synchronisation in plankton distributions in a similar manner. They considered an ensemble of plankton populations, represented by the Nutrient–Phytoplankton–Zooplankton model of Steele and Henderson (1981) with a fixed set of parameter values, coupled via a simple nearest-neighbour flux between patches. By varying the strength of flow between patches and looking at the stability of the fully synchronised state, they were able to establish a critical strength of coupling required for homogeneous dynamics to persist. Two, eight and ten patch ensembles were considered, with results suggesting some dependence of this critical coupling on the number of patches.

A set-up such as that of Hillary and Bees (2004) is a simple parody of a biophysical carbon model: biological dynamics are represented by an ecosystem model common to all grid-cells and the nearest-neighbour coupling approximates the advective and diffusive processes of the physical flow. In many cases, carbon cycle modellers may select a biological model "off-the-shelf" through subjective choice or simply because the model is well-studied. A particular set of biological model parameter values will be chosen, with each parameter subject to a lesser or greater degree of uncertainty. The number of grid-cells used in the simulation will be dictated by a variety of factors such as available computing power, the sampling resolution of empirical data that the simulation hopes to reproduce or, again, subjective choice. Following the approach of Hillary and Bees (2004), the present study therefore aims to address the following question: for oceanographic modelling, what impact does the choice of biological representation at grid-cell level, and the number of grid-cells used, have upon the dynamic features of the fully coupled biophysical system? The results of such a study will be of importance to biophysical modellers.

Specifically, we consider a chain of n grid-cells coupled via a nearest-neighbour flow (with no-flux boundary conditions) designed to approximate mixing processes between adjacent grid-cells. This mixing is a proxy for the effectively diffusive effects of flow at scales smaller than the grid-cell. The biology within each grid-cell is identically represented by a plankton ecosystem model. We consider three different plankton models, which are all typical of those used in the literature to represent upper-ocean biological processes. The models, which will be introduced in Section 2, all represent plankton population dynamics but differ in terms of state variables and functional forms. Within this framework, varying the strength of the flux between grid-cells, we establish the strength of coupling required for the system to exhibit synchronised (spatially homogeneous) dynamics as a function of the choice of (i) biological model, (ii) biological model parameter values and (iii) the number of grid-cells forming the ensemble. This is referred to as the critical coupling.

It is necessary in this preliminary study to consider the simplest possible case; more detailed studies will build on its results. Namely, we consider the case of identical chaotic oscillators: the biology within each grid-cell of the ensemble is represented by the same system of ordinary differential equations and accompanying set of parameter values. Realistically, we would expect spatial and temporal variation in plankton dyamics; for example, phytoplankton growth rates may vary spatially as a result of differences in temperature or species composition. Later studies will need to incorporate such variation. Ecosystem models may exhibit different types of dynamical behaviour, from steady state to limit cycles to chaos,

depending upon the functional forms used to represent biological processes and choice of parameter values (e.g., Edwards and Brindley, 1999). This change in dynamical behaviour is also observed in empirical plankton studies (Fussman et al., 2000). Work has shown that a coupled system of identical oscillators, such as that being considered here, will always synchronise stably if the individual oscillators exhibit steady state or limit cycle solutions (Pikovsky et al., 2001); this is a property that vanishes immediately if we consider *nonidentical* oscillators (representing spatial variation), because the mismatch in representation of each oscillator introduces a desynchronising influence that is lacking in the system of identical oscillators. On the other hand, a system of coupled *chaotic* oscillators has an inherent desynchronising mechanism provided by the exponential divergence of nearby trajectories that is characteristic of a chaotic system (Strogatz, 1994), even when each oscillator is identically represented mathematically. Hence, since identical coupled limit-cycle or steady-state osillators will always stably synchronise, this study focuses on regions of model parameter space for which the models exhibit chaotic dynamics. In particular, we determine the ability of the coupled system to synchronise for the "most chaotic" (i.e. nearby trajectories separate most rapidly) region of parameter space. Behaviour at this most extreme point will then bound the behaviour for the whole of parameter space. The effects of the noise and spatial variation in parameters that would, in the real-world case, be inherent in the system, are not directly studied here. However, future studies will consider the more biologically realistic set-up of non-identically represented patches and so will consider both desynchronising influences.

For the system considered here, of n identically-represented chaotic patches, we show that the critical coupling may be inferred from the dynamic properties of a single grid-cell and the number of grid-cells comprising the ensemble. Consequently, the emergent features of the coupled biophysical model are dependent upon the choice of grid-cell-level biology and the spatial resolution of the simulation.

2. Methods

2.1. The biological models

To reduce typical models of the global ocean carbon cycle to the simplest possible case, we consider an ensemble of effectively diffusively-coupled, biologically-dynamic grid-cells. The population dynamics within each grid-cell, which may be thought of as a region of ocean of, as yet, unspecified length-scale, is represented by a plankton ecosystem model typical of those used in the literature. In particular, we have a chain of n coupled grid-cells, with the plankton population within each grid-cell evolving according to

$$\dot{\mathbf{v}}_\mathbf{i} = F(\mathbf{v}_\mathbf{i}) + \varepsilon\,(\mathbf{v}_{\mathbf{i}-\mathbf{1}}, \mathbf{v}_\mathbf{i}, \mathbf{v}_\mathbf{i} + \mathbf{1}) \cdot \mathbf{q},$$

where each population $\mathbf{v}_\mathbf{i} = (s_1, s_2, \ldots, s_m)$ consists of m species s_j at position i along the chain. ε determines the strength of coupling between grid-cells and

the vector

$$\mathbf{q} = \begin{cases} (1,-2,1) & i \in [2, n-1] \\ (0,-1,1) & i = 1 \\ (1,-1,0) & i = n \end{cases},$$

specifies the coupling configuration, i.e. nearest-neighbour coupling with no-flux boundary conditions.

The function $F(\cdot)$ is the system of differential equations representing the biological evolution of each patch in isolation. The basic biological models selected for this study were first formulated by Steele and Henderson (1981) and Hastings and Powell (1991) (hereafter referred to as SH81 and HP91, respectively), and are typical of those used in biophysical modelling studies of the pelagic ocean (Totterdell, 1993). The models were selected as examples that use different state variables, i.e. representing explicitly different components of the ecosystem, and different functional forms for the trophic interactions. A brief description of the models will be given here, but fuller details may be found in the earlier-mentioned references and in Edwards and Brindley (1996) and Edwards (2001) for SH81 and Caswell and Neubert (1998) for HP91.

Both SH81 and HP91 are zero-dimensional models representing, by a system of autonomous ordinary differential equations, the processes occurring in a physically homogeneous upper ocean layer. SH81 (Eqs. (1)–(3), with parameters given in Table 1), however, contains an implicit, biologically-inactive deeper layer with a fixed nutrient content, which acts by way of vertical mixing as a nutrient source for the upper layer biology.

SH81 models nutrient (N), phytoplankton (P) and zooplankton (Z) concentrations as follows:

$$\begin{aligned} \frac{dN}{dt} &= -\frac{aN}{(e+N)(b+cP)}P + rP + \frac{\zeta\beta P^2}{\mu^2+P^2}Z + \gamma dZ + k(N_0 - N) \\ &= -\text{uptake} + \text{respiration} + Z\,\text{excretion} + Z\,\text{predators excretion} + \text{mixing}, \end{aligned} \tag{1}$$

$$\begin{aligned} \frac{dP}{dt} &= \frac{aN}{(e+N)(b+cP)}P - rP - \frac{\zeta P^2}{\mu^2+P^2}Z - sP - kP \\ &= \text{uptake} - \text{respiration} - \text{grazing by } Z - \text{sinking} - \text{mixing}, \end{aligned} \tag{2}$$

$$\begin{aligned} \frac{dZ}{dt} &= \frac{\zeta\alpha P^2}{\mu^2+P^2}Z - \gamma dZ \\ &= \text{growth due to grazing on } P - \text{higher predation}. \end{aligned} \tag{3}$$

The change in the autotrophic phytoplankton concentration is modelled as the sum of their growth, co-limited by nutrients and light, and losses due to respiration, mixing and sinking out of the upper layer, and grazing by zooplankton. Of the material grazed by zooplankton, a fixed fraction is assimilated, contributing to zooplankton growth. Predation by higher predators closes the food chain from above.

Table 1 Biological model parameters

Parameter	Symbol		Reported range	Chaotic window			Units
	SH81	HP91		SH81	SH81b	HP91	
P growth parameter	a		0.1–0.6	0.198–0.201	0.199–0.201		$m^{-1}\ d^{-1}$
P growth rate		$R \equiv \frac{a}{b}$	0.1–0.6			0.7–3.75	d^{-1}
Light attenuation by water	b		0.04–0.2	0.199–0.203	0.1995–0.2005		m^{-1}
Self-shading by P	c		0.3–1.2	0.37–0.43			$m^2\ gC^{-1}$
P carrying capacity		$K \equiv \frac{2b}{c}$	0.04–0.2			0.28–0.32	m^{-1}
Herbivorous Z mortality	d		0.015–0.15	0.1418–0.1421	0.1401–0.1402		d^{-1}
		d_1				0.09–0.125	d^{-1}
Carnivorous Z mortality		d_2	0.015–0.15			0–0.05	d^{-1}
N half-saturation constant	e		0.02–0.15	0.027–0.04	0.0295–0.0305		$gC\ m^{-3}$
Exchange rate with lower layer	k		0.0008–0.13	0.0499–0.0506	0.0498–0.0502		d^{-1}
P respiration	r		0.05–0.15	0.143–0.157	0.148–0.153		d^{-1}
P sinking	s		0.032–0.08	0.038–0.043	0.039–0.041		d^{-1}
Lower layer N concentration	N_0		0.1–2.0	0.998–1.01	0.998–1.002		$gC\ m^{-3}$
Herbivorous Z	α		0.2–0.75	0.2498–0.2502	0.2499–0.2501		
		c_1				0.39–0.51	
Carnivorous Z growth efficiency		c_2	0.2–0.75			0.4–0.65	
Z excretion fraction	β		0.25–0.8	0.325–0.335	0.328–0.332		
Remineralisation of Z excretion	γ		0.5–0.9	0.49–0.54	0.495–0.507		
Herbivorous Z grazing rate	ζ		0.6–1.4	0.5995–0.6003	0.5998–0.6002		d^{-1}
		a_1				0.48–0.72	d^{-1}
Carnivorous Z grazing rate		a_2	0.6–1.4			0.3–0.75	d^{-1}
Herbivorous Z grazing half-sat. const.	μ		0.02–0.1	0.0347–0.0351	0.0349–0.0351		$gC\ m^{-3}$
		b_1				0.08–0.11	$gC\ m^{-3}$
Carnivorous Z grazing half-sat. const.		b_2	0.02–0.1			0.01–0.16	$gC\ m^{-3}$

Note. Ranges are taken from Edwards and Brindley (1996), wherein values from various studies are collated.

A fixed proportion of the material grazed by zooplankton and higher predators is excreted back to the nutrient pool.

To investigate the effect of a simple change of functional form, leaving choice of state variables and general structure intact, a variation on the above model with alternative nutrient uptake term $\frac{a}{b(e+N)}P$ will also be considered and is hereafter referred to as SH81b. Here, we have a scenario where self-shading by the phytoplankton is assumed to be a negligible component of the light limitation.

The model HP91 was not specifically formulated to represent a plankton ecosystem, rather as a generic three-species food chain, but Caswell and Neubert (1998) and Srokosz et al. (2003) applied the model to a plankton ecosystem by taking the three trophic levels to represent phytoplankton, herbivorous zooplankton (H) and carnivorous zooplankton (C) components:

$$\begin{aligned}\frac{dP}{dt} &= RP\left(1-\frac{P}{K}\right)-\frac{a_1PH}{b_1+P}\\ &= \text{logistic growth} - \text{grazing by } H, \qquad (4)\\ \frac{dH}{dt} &= \frac{c_1a_1PH}{b_1+P}-\frac{a_2HC}{b_2+H}-d_1H\\ &= \text{growth due to grazing on } P - \text{grazing by } C - \text{natural mortality}, \qquad (5)\\ \frac{dC}{dt} &= \frac{c_2a_2HC}{b_2+H}-d_2C\\ &= \text{growth due to grazing on } H - \text{higher predation}, \qquad (6)\end{aligned}$$

with parameter values given in Table 1.

In HP91, carnivores are explicitly modelled and nutrient concentrations are not; that is, nutrients are taken to be non-limiting to phytoplankton growth. The model is somewhat simpler than SH81 in that recycling processes are not considered, so that the fundamental flow structure differs. Phytoplankton population increases according to logistic growth, limited by a carrying capacity, and decreases due to grazing by herbivores, which are, in turn, grazed by carnivores. At each trophic level, a fixed proportion of grazed material is assimilated and the rest lost from the system. Herbivores and carnivores are each subject to a linear natural mortality term. SH81/SH81b and HP91 represent different interpretations of the planktonic ecosystem: SH81 and SH81b are built on the assumption of bottom-up control; HP91 is built on the assumption of top-down control.

Historically, plankton modellers have settled upon a variety of functional forms to describe the interactions between the components of the ecosystem, and the previously mentioned models are no exception. In order to make the models as directly comparable as possible, we can relate the parameters from the different functional forms in such a way that a similar range of values for that process can be used.

The model HP91 contains functions for growth, grazing and mortality, of which only the latter is of an equivalent form in SH81. In SH81, autotrophic growth is taken to be co-limited by nutrients, in the Michaelis–Menten form, and light

availability. Growth takes maximum value $\frac{a}{b}$ at $P = 0$ in the limit as N tends to infinity. HP91 assumes logistic growth, limited by a carrying capacity. This has maximum value R, again at $P = 0$. Taking $R \equiv \frac{a}{b}$, we therefore set the models to have the same intrinsic maximum growth rate.

Taking nutrients to be non-limiting in the growth rate term of HP91, so that growth is limited by self-shading by the phytoplankton themselves, then the term $R(1 - \frac{P}{K})$ may be equated with the self-shading component of the SH81 growth rate term. Since we have $R \equiv \frac{a}{b}$, this leads us to compare $1 - \frac{P}{K}$ and $\frac{b}{b+cP}$. We may then equate half-saturation constants of these two forms: $\max(1 - \frac{P}{K}) = 1$, half of which is attained at $P = \frac{K}{2}$. Similarly, $\max(\frac{b}{b+cP}) = 1$, half of which is attained at $P = \frac{b}{c}$. Equating these two, we get $K \equiv \frac{2b}{c}$.

Grazing terms, although different, are formulated in both models in terms of the half-saturation constant (ζ and a_i), the maximum grazing rate (μ and b_i) and the assimilation coefficient (α and c_i), making each of these parameters directly relatable.

Table 1 summarises the previous discussion. Reported parameter ranges are as collated by Edwards and Brindley (1996) in their study of SH81.

2.2. *Single grid-cell dynamics*

Both models, under variation of parameter values within the reported ranges (see Table 1), are known to exhibit steady state, limit cycle and chaotic dynamics. It is necessary to quantify this behaviour because, as explained later, the behaviour of the individual grid-cell, as described by the biological model, impacts upon the fully coupled system. An indication of the behaviour may be obtained by calculating the *Lyapunov characteristic exponent*, which measures the exponential rate of separation of nearby trajectories of the system in phase space. An m-dimensional dynamical system will have m Lyapunov exponents, quantifying the separation rate in all m directions of movement, but it is the largest Lyapunov exponent that indicates the kind of dynamics to be expected. A positive largest Lyapunov exponent indicates that there is at least one direction in which exponential separation rather than convergence of nearby trajectories in phase space can occur, leading to chaos in a dynamical system (Strogatz, 1994). If the largest Lyapunov exponent is zero or negative, then the system will exhibit limit cycles or steady states, respectively. We calculate a finite-time approximation of the largest Lyapunov exponent λ of a dynamical system using the following method:

The system is integrated until transients have died and we are 'on' the attractor. The trajectory ($\mathbf{u}$) on the attractor will be a 'reference' trajectory. We then use a 'test' trajectory ($\mathbf{w}$), which at time t_0 is set a small distance d_0 from $\mathbf{u}$, to examine the rate at which nearby trajectories diverge.

If S_{i-1} denotes the amount by which the original perturbation has been 'stretched' at iteration step $i - 1$, then the exponential rate of divergence λ_i is given by

$$S_{i-1} = e^{\lambda_{i-1} t_{i-1}}.$$

Let dS denote the stretch experienced over the next time step. Then

$$S_i = e^{\lambda_i t_i} = e^{\lambda_{i-1} t_{i-1}} dS,$$

and, taking logs of both sides and dividing by t_i, we obtain

$$\lambda_i = \frac{\lambda_{i-1} t_{i-1} + \log dS}{t_i},$$

as a finite-time estimate of the Lyapunov exponent λ, so that λ can be calculated iteratively.

In the case of chaotic behaviour, the distance between the two trajectories quickly becomes too large for the definition of λ (as the growth of the distance between two initially *close* trajectories) to be valid. To avoid this problem, we rescale the distance to $\mathbf{u}$ at each time-step, preserving the direction of the vector but restoring the distance between $\mathbf{u}$ and $\mathbf{w}$ to d_0,

$$\mathbf{w}_{\text{new}} = \mathbf{u} + \frac{\mathbf{w} - \mathbf{u}}{dS}.$$

The process of iteration and rescaling is repeated until λ has converged. λ may be calculated for a range of values of a specified biological model parameter, allowing the occurrence of chaos or limit cycles to be tracked within a biologically acceptable range of parameters.

2.3. Ensemble dynamics

The coupled system is *synchronised* if the dynamics resides on the region of phase space contained within the *synchronisation manifold*

$$\mathcal{M}_s = \{v_1, v_2, \ldots, v_n | v_1(t) = v_2(t) = \cdots = v_n(t)\}.$$

On perturbation from synchrony, the evolution of the coupled ensemble of grid-cells may return to synchrony (become spatially homogeneous) or remain unsynchronised (spatially patchy), depending on the dynamics of the individual grid-cells and the strength of coupling between them.

By analogy to the real world, where a plankton "patch" is a region of sea of homogeneous plankton biomass, we may consider a model plankton "patch" to be a synchronised subset of grid-cells C_k, $1 \leq k \leq n$. However, the system considered here – that of an ensemble of identically represented oscillators – is capable of exhibiting only two system-level stable states as the coupling strength is increased: complete asynchrony ($k = 1$) or complete synchrony ($k = n$); if the coupling strength is sufficient for synchrony then as soon as two adjacent oscillators become synchronised they are, since they are identically represented, locked into that state and thereafter act as one oscillator, leading eventually to synchrony of all oscillators. Alternative set-ups, such as ensembles of non-identical oscillators, allow

stable dynamics with $1 < k < n$, a phenomenon referred to as *clustering*(Belykh et al., 2003).

The stability of the fully synchronised state is established by calculating the largest *normal (or transverse) Lyapuov exponent* Λ; that is, the rate of growth of perturbations away from synchrony in the direction transverse to the synchronisation manifold.

We have a chain of n-coupled plankton grid-cells $\mathbf{v_1}, \mathbf{v_2}, \ldots, \mathbf{v_n}$ and wish to determine the rate of expansion of a perturbation away from the synchronous state $\mathbf{v_1} = \mathbf{v_2} = \cdots = \mathbf{v_n}$, which resides on $\mathcal{M}_s$. To enable the separation of dynamics *on* and *normal* to $\mathcal{M}_s$, a change of variables from the set $\mathbf{v_1}, \mathbf{v_2}, \ldots, \mathbf{v_n}$ of grid-cells to an orthogonal set $\pi_1, \pi_2, \ldots, \pi_n$ is applied such that $\pi_2 = \pi_3 = \cdots = \pi_n = 0$ when the populations are synchronised, and π_1 represents the dynamics on the synchronous attractor; for example, as follows,

$$\begin{pmatrix} \pi_1 \\ \pi_2 \\ \vdots \\ \vdots \\ \pi_n \end{pmatrix} = \frac{1}{n} \begin{pmatrix} 1 & \cdots & \cdots & \cdots & 1 \\ 1 & \cdots & \cdots & 1 & -(n-1) \\ 1 & \cdots & 1 & -(n-2) & 0 \\ \vdots & & & & \vdots \\ 1 & -1 & \cdots & \cdots & 0 \end{pmatrix} \begin{pmatrix} \mathbf{v_1} \\ \mathbf{v_2} \\ \vdots \\ \vdots \\ \mathbf{v_n} \end{pmatrix}.$$

As with the calculation of Lyapunov exponents described earlier, a single uncoupled oscillator is initially integrated until transient behaviour dies and dynamics lie on the synchronisation manifold, with values π_0. For a reference trajectory $\mathbf{u} \in \mathcal{M}_s$, we set

$$\mathbf{u} = (\pi_0, 0, \ldots, 0).$$

Since $\mathcal{M}_s$ is invariant, the reference trajectory $\mathbf{u}$ remains within $\mathcal{M}_s$ for all time. A test trajectory $\mathbf{w}$ is initiated by adding a small initial perturbation away from synchrony of magnitude d_0 ($\mathcal{O}(10^{-5})$) to trajectory $\mathbf{u}$ so that

$$\mathbf{w} = \mathbf{u} + \left(0, \frac{d_0}{\sqrt{n-1}}, \ldots, \frac{d_0}{\sqrt{n-1}}\right),$$

i.e. a perturbation normal to $\mathcal{M}_s$.

Both trajectories are integrated forward for a few time-steps and the extension $dS_\perp$ from synchrony normal to the synchronisation manifold relative to the original perturbation d_0 is given by

$$dS_\perp = \frac{\sqrt{\sum_{j=2}^{n} (\mathbf{w_j} - \mathbf{u_j})^2}}{d_0},$$

where $\mathbf{u_j}$ and $\mathbf{v_j}$ are the jth components of the reference and test trajectories at time t, respectively. The finite-time transverse Lyapunov exponent at iteration step

i is then

$$\Lambda_i = \frac{\Lambda_{i-1} t_{i-1} + \log(dS_\perp)}{t_i},$$

measuring the stretch *in the direction transverse to synchrony* of the initial perturbation with time.

The process is repeated until convergence of Λ is achieved. However, as with the calculation of λ described earlier, in the case of chaotic orbits the separation quickly becomes too large for us to be considering *nearby* trajectories. Again, a rescaling must be applied to avoid this problem.

If $\Lambda < 0$, then the synchronous state is stable since perturbations from synchrony will decay. This is a threshold phenomenon; it depends upon the magnitude of coupling and there exists a critical strength of coupling above which synchrony will re-establish itself after perturbation. In other words, there exists critical coupling $\varepsilon = \varepsilon_c$ such that $\Lambda(\varepsilon_c) = 0$.

Theory (Fujisaka and Yamada, 1983) shows that ε_c is directly proportional to the largest Lyapunov exponent λ of the dynamics in an *individual* grid-cell. Therefore, in order to place an upper bound on ε_c for each model, it is required to find where λ attains its maximum within the reported range of parameters. Since $\lambda = 0$ in non-chaotic regions of parameter space, $\varepsilon_c = 0$, and therefore a coupled system of non-chaotic identical oscillators will always stably synchronise. We therefore only need consider chaotic regions of parameter space, identified by $\lambda > 0$, and look for the "most chaotic" point, i.e. where λ attains its maximum.

An iterative method is used to find an approximation of the maximum value of λ as a function of the biological model parameters. Each biological model has a set $\Omega = \{a_1, a_2, \ldots, a_l\}$ of l parameters. Since $\lambda = 0$ for steady-state and limit cycle dynamics, we need only consider chaotic regions. We initiate the algorithm at a point $\mathbf{a}(0) = (a_1(0), a_2(0), \ldots, a_l(0)) \in \Omega$ for which the model exhibits chaos. Such a point is known to exist for SH81 from the work of Edwards and Brindley (1999); for HP91 chaotic regions are clearly demonstrated in the original paper.

For each parameter a_j, we have a biologically-plausible range $[a_{j_{\min}}, a_{j_{\max}}]$ (see Table 1), giving an l-dimensional hypercube bounded by the $a_{j_{\min}}$ and $a_{j_{\max}}$, for $j = 1, \ldots, l$, containing the initial point $\mathbf{a}(0)$. For each step i of the iteration, and for each parameter a_j of the set, λ is calculated with parameters $a_k(i)$, $k < j$, and $a_k(i-1)$, $k > j$, fixed for $k \neq j$ and parameter a_j varied across the range $[a_{j_{\min}}, a_{j_{\max}}]$. The value of $a_j(i)$ is then set as the value within $[a_{j_{\min}}, a_{j_{\max}}]$ giving maximum λ. This is repeated for all parameters a_j, giving a new parameter set $\boldsymbol{a}(i)$. If inspection of these "slices" across parameter space indicates that

$$\begin{aligned}
&\max_{a_1 \in [a_{1_{\min}}, a_{1_{\max}}]} \lambda\,(a_1, a_2(i), a_3(i), \ldots, a_l(i)) \\
&\approx \max_{a_2 \in [a_{2_{\min}}, a_{2_{\max}}]} \lambda\,(a_1(i), a_2, a_3(i), \ldots, a_l(i)) \\
&\vdots \\
&\approx \max_{a_l \in [a_{l_{\min}}, a_{l_{\max}}]} \lambda\,(a_1(i), a_2(i), a_3(i), \ldots, a_l)
\end{aligned},$$

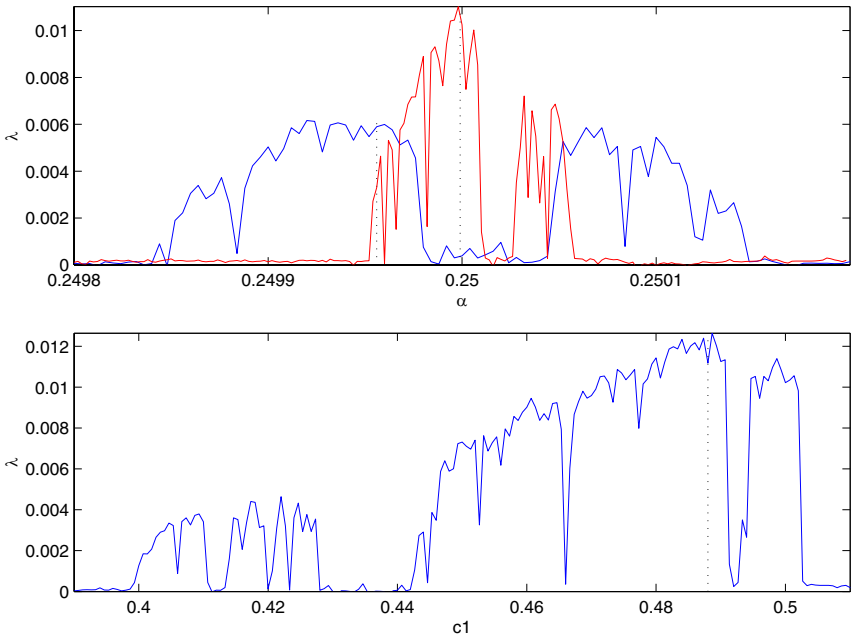

Fig. 1 *Parameter space:* Largest Lyapunov exponent λ calculated across the chaotic windows for herbivorous zooplankton growth efficiency parameters α (SH81 in *blue*; SH81b in *red*) and c_1 (HP91). All other parameters are held at those giving maximum largest Lyapunov exponent λ. *Dotted lines* indicate the parameter values giving λ_{max}. The calculations are shown only across the chaotic regions of parameter space, since $\lambda = 0$ for equilibrium and limit cycle regions.

to within a specified level of accuracy, then the parameter values giving the approximate maximum λ are judged to have been found (see Fig. 1 and Table 1). Otherwise, the process is repeated for step $i + 1$.

It is possible that the approximate method detailed here may miss the chaotic apex of a model. For example, a disconnected region of chaotic parameter space may exist that does not intersect with the parameter "slices" through the initial chaotic point. No such isolated chaotic regions were found during investigation of the models using the dynamical systems package AUTO. An exhaustive search of the l-dimensional parameter space of the models considered here would be extremely computationally expensive. The method is therefore considered a good necessary approximation for the most chaotic point within biologically acceptable bounds. Of course, the global apex for the model may lie outside these bounds.

3. Results

3.1. Single grid-cell

The iterative method described earlier was used to find the region of parameter space giving the maximum largest Lyapunov exponent λ for each model. As

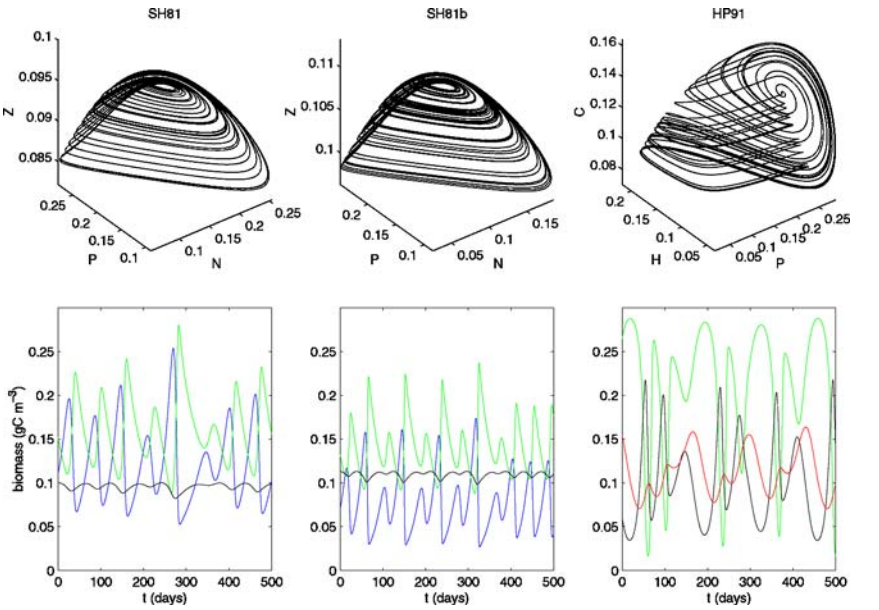

Fig. 2 *Model dynamics:* Phase space attractors and temporal evolution of state variables for SH81 (*left*), SH81b (*middle*) and HP91 (*right*). Parameter values set to those giving maximum largest Lyapunov exponent λ. Transient dynamics not shown. Key: *blue* – nutrients, *green* – phytoplankton, *black* – herbivorous zooplankton, *red* – carnivorous zooplankton.

an example, Fig. 1 shows how λ varies as a function of herbivorous zooplankton growth efficiency across 'slices' of parameter space for all three models; all other parameters are kept constant at the established λ apex. Because $\lambda > 0$ only where dynamics are chaotic, Fig. 1 shows calculations only across the chaotic regions of parameter space. However, since this a necessarily finite-time calculated approximation of a quantity defined for infinite-time, the exponent does not quite go to 0 in the limit-cycle and steady-state regions. Chaotic ranges established in this way for all other model parameters are included in Table 1. The global chaotic apex for the model HP91 lies outside the suggested parameter ranges. For this reason, we consider two apices for this model: the points in parameter space giving maximum λ *inside* and *outside* suggested ranges, respectively.

λ_{max} (denoted by dotted lines in Fig. 1) is approximately 0.0063 d^{-1} and 0.01 d^{-1} for models SH81 and SH81b, respectively. Constrained to suggested parameter ranges, HP91 has apex 0.011 d^{-1}; λ_{max} reaches 0.013 d^{-1} if parameters are allowed to vary beyond these ranges. Model dynamics at these points in parameter space, both as a time series and in phase space, are shown in Fig. 2.

3.2. Two-patch stability

Figure 3 shows the calculated transverse Lyapunov exponent, Λ, for a two grid-cell coupled system as a function of varying strength of coupling ε for each model.

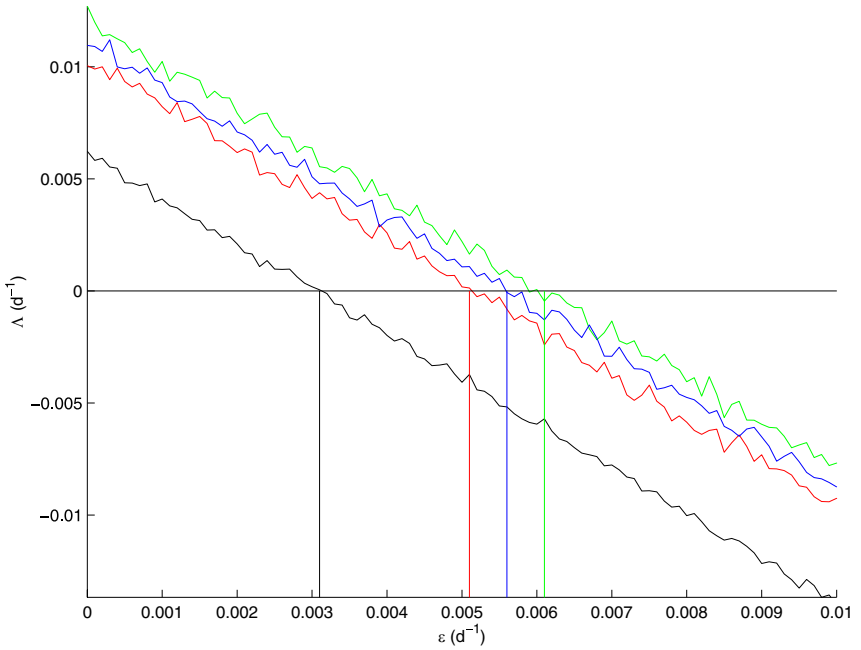

Fig. 3 *Critical coupling strength:* Calculated largest normal Lyapunov exponent Λ as a function of coupling strength ε for models SH81 (*black*), SH81b (*red*), HP91 restricted to suggested parameter ranges (*blue*) and HP91 not restricted to suggested parameter ranges (*green*). Model parameters set at values giving maximum largest Lyapunov exponent λ. Critical coupling strength ε_c indicated by value of ε giving $\Lambda(\varepsilon) = 0$.

The coupling strength at which $\Lambda(\epsilon)$ changes from positive (perturbations from synchrony grow) to negative (such perturbations decay) is the critical coupling strength ε_c required for stable synchrony. ε_c is seen to equal 0.0031 d^{-1}, 0.0051 d^{-1}, 0.0061 d^{-1} and 0.0056 d^{-1} for models SH81, SH81b, HP91 (outside) and HP91 (inside), respectively. Since theory (Fujisaka and Yamada, 1983) shows that ε_c is directly proportional to λ for this type of coupling, and we have established $\lambda_{\max}$ within parameter space, $\varepsilon_c(\lambda_{\max})$ gives an upper bound on ε_c for each model: a coupling strength of $\varepsilon > \varepsilon_c(\lambda_{\max})$ is sufficient to stably synchronise the two-grid-cell coupled system for any set of biological parameter values. As an example, using the model SH81, Fig. 4 shows how system dynamics differ below and above this 'blowout bifurcation' (as the parameter ε moves below the critical point, the stability of the synchronous state is 'blown out'). We initiate the integration with the two coupled patches out of synchrony with one another, so that $|\mathbf{v_1} - \mathbf{v_2}| = \delta > 0$ where δ is a small perturbation from synchrony. In Fig. 4, the evolution of this perturbation, for the phytoplankton components P_1 and P_2 of the two patches, is plotted with time for a coupling strength of $\varepsilon < \varepsilon_c$ (top) and $\varepsilon > \varepsilon_c$ (bottom). It is seen that a coupling strength of 0.0025 d^{-1}, which is below ε_c, is insufficient to restore synchrony, so that the system displays heterogeneous dynamics. A coupling of 0.0035 d^{-1} is strong enough to draw the oscillators back into synchrony.

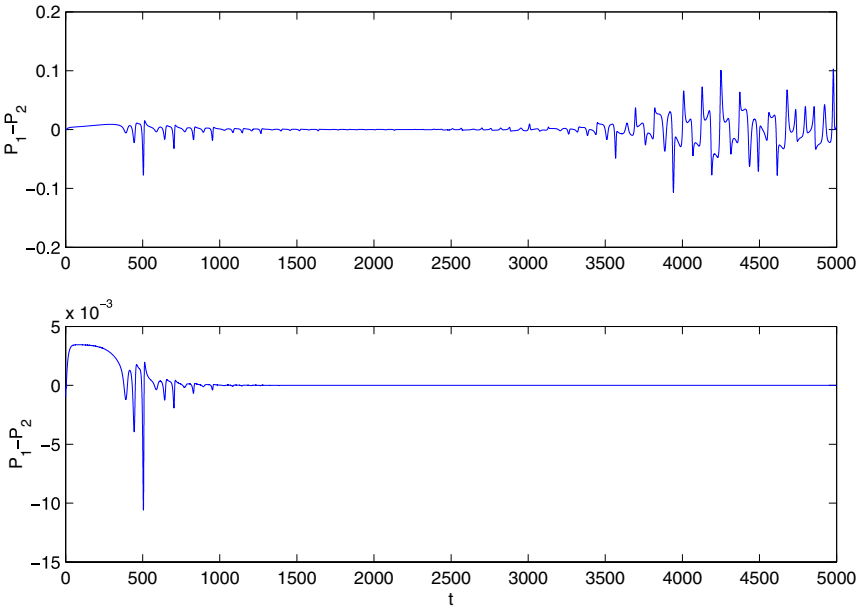

Fig. 4 *Two-patch dynamics:* Time evolution of difference between phytoplankton components P_1 and P_2 plotted for coupling strength $\varepsilon = 0.0025$ ($<\varepsilon_c$) and $\varepsilon = 0.0035$ ($>\varepsilon_c$) in top and bottom panels, respectively. Model used is SH81 and parameters are set at values giving maximum largest Lyapunov exponent λ.

The results in Fig. 3 fit well with the predictions of Fujisaka and Yamada (1983). For a two-grid-cell system, the theory states that $\varepsilon_c = \frac{\lambda}{2}$. Using calculated λ, this gives predicted critical coupling strengths of $0.0032\,\mathrm{d}^{-1}$, $0.0048\,\mathrm{d}^{-1}$, $0.0065\,\mathrm{d}^{-1}$ and $0.0055\,\mathrm{d}^{-1}$ for models SH81, SH81b, HP91 (outside) and HP91 (inside), respectively. Figure 5 gives an example of how well the empirical and theoretical results match for a cross section through parameter space; for model SH81, calculated ε_c is plotted along with $\frac{\lambda}{2}$ for the phytoplankton growth rate parameter a varied across the chaotic window of parameter space, keeping all other parameters at λ apex values. This clearly illustrates the dependence of the critical coupling strength upon the parameter values, and therefore dynamics, of the isolated model in an individual grid-cell.

3.3. n-patch stability

Next considered was a chain of n-coupled grid-cells, with nearest-neighbour coupling and the biology in each patch represented by the SH81 model. ε_c was established as a function of n: firstly, by direct computation and, secondly, by using the calculated values of $\lambda_{\max}$ to apply the theory of Fujisaka and Yamada (1983).

The results are plotted in Fig. 6. It is seen that the critical coupling strength increases with the length of the chain, so that a greater strength of mixing between patches is needed to synchronise a chain with more patches. Additionally, we see

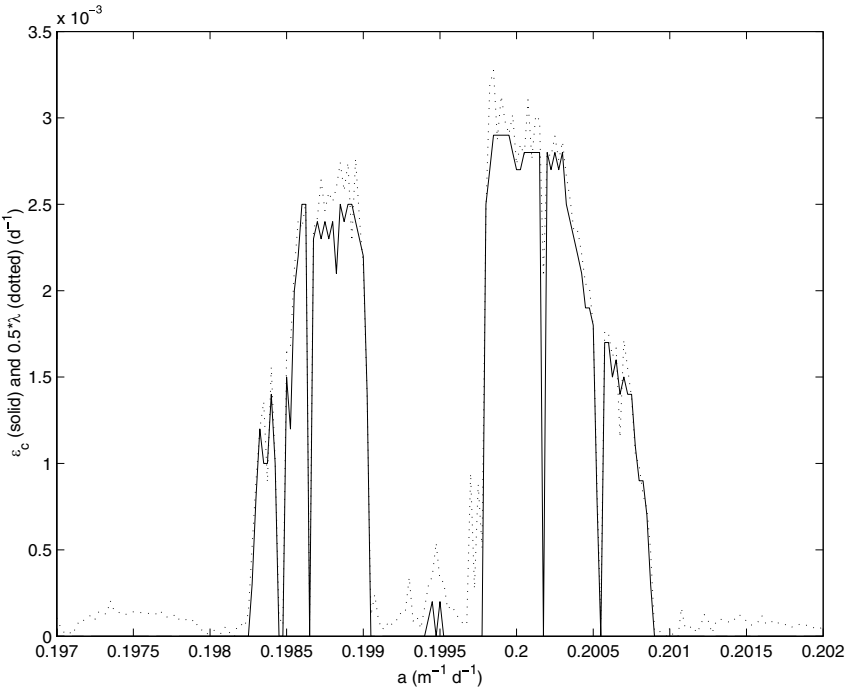

Fig. 5 *Comparison with theory of Fujisaka and Yamada (1983):* Calculated critical coupling strength ε_c (*solid line*) and half-largest Lypaunov exponent λ (*dotted*) plotted across chaotic window for model SH81 phytoplankton growth parameter a.

that the theory of Fujisaka and Yamada (1983), which states that the critical coupling strength is related to chain length and largest Lyapunov exponent λ of the single-patch biological model as

$$\varepsilon_c = \frac{\lambda}{\min_{k=1,\ldots,n-1}\left(4\sin^2\left(\frac{k\pi}{2n}\right)\right)} \tag{7}$$

agrees well with the computed values.

It is evident that a prediction of ε_c for a system of this type with any number of grid-cells may be inferred from knowledge of the Lyapunov exponent of the isolated biological model in any one grid-cell.

Although n-patch results have been presented here for a chain of patches each represented by the SH81 model, the same results are obtained with the other models considered.

4. Discussion

To address the question of how grid-cell biology and the number of grid-cells impacts upon the behaviour of coupled biophysical simulations, we applied the

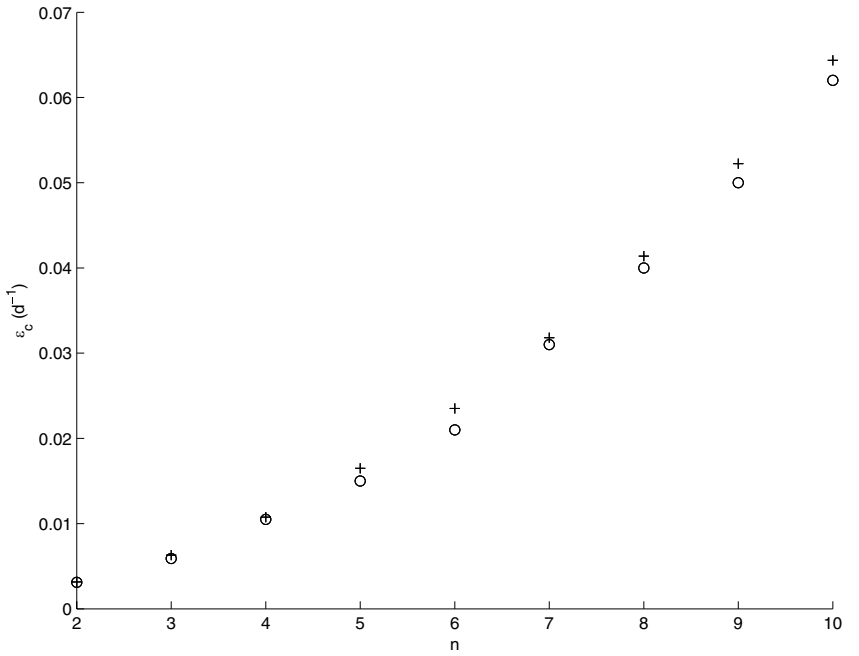

Fig. 6 *n-patch chain:* Critical coupling strength ε_c as a function of number of patches n. Each patch is represented by SH81 model and the chain has fixed-ends. *Crosses* indicate Λ as predicted by Fujisaka and Yamada (1983). *Circles* indicate experimental results for 3, 4, 5 and 10-patch chains.

methods of sychronisation theory to an ensemble of identically-represented interacting plankton populations. Using several different typical plankton ecosystem models to represent the evolution of each patch, and varying the number of patches comprising the ensemble, we calculated the critical strength of patch-to-patch coupling required for stably synchronous dynamics to occur. The study focused on chaotic regions of parameter space since identical steady-state and limit cycle oscillators always stably synchronise.

4.1. Critical coupling strength for synchrony

For a chain of n-coupled plankton grid-cells, each represented by the same biological model, the strength of coupling ε_c required for stably homogeneous (synchronised) dynamics to occur is found to vary as a function of biological model, model parameters and n. In fact, results bear out the theory of Fujisaka and Yamada (1983) as in Eq. (7).

We see that the critical coupling varies linearly with λ, implying that the use of "more chaotic" biological dynamics at grid-cell level reduces the ability of the chain to exhibit homogeneous dynamics. More significantly, ε_c increases with n. In other words, a stronger mixing between grid-cells is required to synchronise a longer chain.

The relationship between ε_c and n can be established as follows. As n becomes large, $\frac{\pi}{2n}$ becomes small and, therefore,

$$\varepsilon_c \approx \frac{\lambda n^2}{\pi^2} \tag{8}$$

(because $\sin(x) \approx x$ for small x) so that the critical coupling increases as n^2.

This has implications for modelling studies. Suppose we wish to model the dynamics of a particular transect of ocean of length L, perhaps to compare the results with observed data. For the purposes of simulation, the transect is divided into a number of grid-cells, depending on various factors such as available computing power and the spatial resolution of the observed data. A plankton ecosystem model is chosen to describe the biology in each grid-cell. To simulate the physical flow, we impose a fixed effectively diffusive coupling of strength ε between grid-cells. Since $\varepsilon_c \propto \frac{\lambda n^2}{\pi^2}$, we know that, for a fixed ε and fixed biological model, there exists a corresponding critical number of grid-cells n_c such that the use of a number of grid-cells $n > n_c$ to divide up the transect L will lead to unsynchronised dynamics. Therefore, the resolution chosen for the simulation of a particular region of ocean could drastically alter the results in a discontinuous manner, as it sets the number of grid-cells used.

As explained, this threshold phenomenon occurs only when the individual grid-cell dynamics are chaotic. That an ensemble of identical chaotic oscillators may have emergent characteristics that bifurcate in this manner is a case against using chaotic plankton ecosystem models in a system like this to study plankton patchiness. This is worrying in the light of recent findings by Gross et al. (2006) that chaotic parameter ranges exist generically in food chains of greater than three components. The model of Hastings and Powell (1991), in particular, contains interspersed windows of chaotic and periodic behaviour throughout its parameter space (as illustrated by Caswell and Neubert (1998) and see also Fig. 1), which in the context of the results of this study might make it unsuitable for use in a coupled biophysical model.

More generally, the results illustrate that the choice of biological model at grid-cell level can have a significant impact at system level. It is noteworthy that SH81b, although differing from SH81 only by a small change of functional form and having similar parameter values and almost identical structure, exhibits chaos over smaller sized regions of parameter space and attains a larger "degree of chaos," as measured by a greater $\lambda_{\max}$ (Fig. 1), which, in turn, reduces the ability of coupled SH81b oscillators to synchronise (Fig. 3). Why the small change to functional form should make a large difference and whether this is of biological significance is not known and would, since the models represent distinct biological scenarios, be a valid line of future enquiry. HP91, despite differing greatly in structure from SH81, has a similar $\lambda_{\max}$ and therefore synchronising ability. For all three models, λ, and therefore ε_c, varies greatly across parameter space. We conclude from this that choice of biological model and parameter set affects the system-level dynamics.

4.2. Critical spatial scale for plankton patchiness

In their study of synchronisation in ensembles of plankton populations, Hillary and Bees (2004) used the empirical relationship between spatial scale l and effective diffusivity $D(l)$ (Okubo, 1971) to relate the critical coupling strength ε_c to an emergent critical length-scale for patchiness in plankton. The observations of Okubo show that for $D(l)$ in $\mathrm{cm}^2\,\mathrm{s}^{-1}$ and l in cm

$$D(l) \approx 0.01 l^{1.15}.$$

Hillary and Bees (2004) consider a chain of length L consisting of n-coupled grid-cells, giving a grid-cell length-scale $\Delta = \frac{L}{n}$. They then equate the diffusive coupling ε with diffusive processes between grid-cells, so that $\varepsilon(l) \approx \frac{D(l)}{\Delta^2}$, where $\frac{1}{\Delta^2}$ approximates the second-order spatial derivative. Using the relationship of Okubo, and taking l as the patch length-scale this gives

$$\varepsilon \approx 0.01 \Delta^{-0.85}.$$

For their eight-grid-cell system, Hillary and Bees (2004) found a critical coupling strength of $0.0075\,\mathrm{d}^{-1}$. Using the relationship mentioned earlier, they equated this with a critical length-scale L_c of around 100 km. Since with increasing length-scale the diffusivity according to the Okubo relationship increases and the appropriate coupling strength decreases, an eight-grid-cell system of length $L > L_c$ will have a diffusivity-related coupling strength $\varepsilon < \varepsilon_c$ and unsynchronised dynamics will result. L_c therefore represents a upper bound on the scale at which we expect to see synchronised patches for a fixed number of grid-cells.

However, we have seen in this study that $\varepsilon_c \propto n^2$ and from the earlier discussion we know $\varepsilon \propto L^{-0.85} n^{0.85}$, so we have a relationship between the number of grid-cells and the critical length-scale:

$$L_c^{-0.85} \propto n^{1.15}.$$

Hence, as Hillary and Bees (2004) in fact predict, the critical length-scale found using this method is a function of the number of grid-cells and therefore resolution of the simulation. As discussed earlier, the model resolution may be dependent upon such arbitrary factors as available computing power. Although we can establish a critical length-scale for a given number of grid-cells, in many cases this relationship can therefore tell us little about the scale at which plankton patches should synchronise, because only the number of grid-cells into which a study region is partitioned, and not the true length-scale, has an effect on whether synchronisation will occur.

The previous discussion depends upon assumptions about the length-scale taken in the approximation of the effective diffusivity. Since, in the work by Okubo (1971), the length-scale is arbitrarily set to a value such that a circle of that radius would contain 95% of the dye material, our patch length-scale Δ as used here is a

natural choice. However, we expect in the case of synchronisation for information to diffuse over the full system, so that the system length-scale L or an intermediate value may be more appropriate. If we set $l = L$, we obtain

$$\varepsilon \approx 0.01\, n^2\, L^{-0.85}$$

so that, upon application of Eq. (8), the n^2 terms cancel to give a constant L_c.

Additionally, care must be taken with our treatment of Eq. (7), where we have taken n to be large. For a fixed system length-scale L, increasing n leads to decreasing Δ. The Okubo (1971) paper deals with a closed range 30 m to 100 km of spatial scales, so that we may reach a value of Δ for which this relationship is not valid.

4.3. Impact on biophysical modelling

To illustrate the impact of these results on physical quantities that may be derived from biophysical models, we examined the effect of synchrony on total primary production (TPP), a quantity frequently estimated from such models. For the example case of a 10-grid-cell chain of SH81 oscillators with parameter values set at the chaotic apex, we calculated TPP as a function of time for (i) a coupling strength of $\varepsilon = 0$ (representing for non-identical initial conditions the "most asynchronous" state achievable) and (ii) $\varepsilon > \varepsilon_c$.

As a function of time, it was found that synchrony increased and decreased the values of TPP attained at maxima and minima, respectively – an effect caused by the additive affect of the concurrent nature of these events in the synchronous case: maximum and minimum TPP were for (i) $0.84\,\mathrm{gC\,m^{-3}\,d^{-1}}$ and $1.03\,\mathrm{gC\,m^{-3}\,d^{-1}}$ and for (ii) $0.67\,\mathrm{gC\,m^{-3}\,d^{-1}}$ and $1.29\,\mathrm{gC\,m^{-3}\,d^{-1}}$ (to 2 d.p.). The mean TPP, however, was found to be around $1\,\mathrm{gC\,m^{-3}\,d^{-1}}$ for both (i) and (ii).

These results, while only qualitative in nature as we are not modelling the seasonal cycle, indicate the need for directing major effort into the understanding of more realistic biophysical models. Otherwise, our confidence in the bulk properties derived from them will be diminished.

5. Conclusions and future considerations

This study has shown that the choice of grid-cell level biology has a direct impact on the ability of a coupled biophysical simulation to exhibit spatially homogeneous dynamics. More alarmingly, we have shown that system-level behaviour can alter in a discontinuous manner as a function of the number of grid-cells. Carbon cycle modelling studies should take these effects into consideration. Furthermore, the results suggest that chaotic ecosystem models should be used with caution to guard against spurious or misleading emergent features. Since the extent of chaotic regions of parameter space has not been determined for plankton models, this is an important result. For SH81, the parameter space appears to contain only relatively small chaotic regions, so that the effect may be of minor concern, whereas HP91 is an example of a model exhibiting chaotic regions spanning most of parameter space.

It is important to stress that this is a preliminary study of the synchronising properties of coupled plankton patches. It has been necessary to consider the simplest possible case, that of identical oscillators. This study provides the basis for future work which will build on the results by considering the impact of both environmental noise and spatially varying properties on the ability of patches to synchronise. The use of non-identical oscillators, both chaotic and periodic, in a system of coupled patches prevents the occurrence of full synchronisation. However, a much richer array of behaviour of approximate synchronisation is then possible, which we refer to as *generalised synchronisation* (see Pikovsky et al. (2001) and the references therein). This less rigid definition requires that there exist a continuous one-to-one mapping relating the dynamics of the oscillators. For example, *phase synchronisation* may occur, where oscillator phases are locked but amplitudes remain uncorrelated. Additionally, for intermediate coupling strengths, a stable state of clustering may occur where the system groups into subsets of synchronised grid-cells (Belykh et al., 2003), i.e. "patches" larger than the size $\frac{L}{n}$ of an individual grid-cell and smaller than the size L of the full system. This type of behaviour has been shown to occur in observed data (e.g., Elton and Nicholson, 1942) and in models similar to that used in this study to model a plankton distribution. If systems of non-identical oscillators are found to exhibit the same kind of phenomena as found here in systems of identical oscillators, then there will be significant impacts on the modelling of spatial variablility in ecosystems.

Acknowledgements

EJG is grateful for an Environmental Mathematics and Statistics (EMS) Programme Studentship funded jointly by NERC and EPSRC.

References

Abraham, E., 1998. The generation of plankton patchiness by turbulent stirring. Nature 391, 577–580.

Bainbridge, R., 1956. The size, shape and density of marine phytoplankton concentrations. Biol. Rev. 32, 91–115.

Belykh, I., Belykh, V., Nevidin, K., Hasler, M., 2003. Persistent clusters in lattices of coupled nonidentical chaotic systems. Chaos 13(1), 165–178.

Blasius, B., Stone, L., 2000. Nonlinearity and the Moran effect. Nature 406, 846–847.

Caswell, H., Neubert, M.G., 1998. Chaos and closure terms in plankton food chain models. J. Plankton Res. 20(9), 1837–1845.

Edwards, A.M., 2001. Adding detritus to a nutrient–phytoplankton–zooplankton model: A dynamical systems approach. J. Plankton Res. 23(4), 389–413.

Edwards, A.M., Brindley, J., 1996. Oscillatory behaviour in a three-component plankton population model. Dyn. Stab. Syst. 11(4), 347–370.

Edwards, A.M., Brindley, J., 1999. Zooplankton mortality and the dynamical behaviour of plankton population models. Bull. Math. Biol. 61, 303–339.

Elton, C., Nicholson, M., 1942. The ten-year cycle in numbers of the lynx in Canada. J. Anim. Ecol. 11(2), 215–244.

Fujisaka, H., Yamada, T., 1983. Stability theory of synchronized motion in coupled-oscillator systems. Prog. Theor. Phys. 69, 32–48.

Fussman, G.F., Ellner, S.P., Shertzer, K.W., Hairston, N.G. Jr., 2000. Crossing the Hopf bifurcation in a live predator–prey system. Science 290(5495), 1358–1360.

Grenfall, B.T., Wilson, K., Finkenstädt, B.F., Coulson, T.N., Murray, S., Albon, S.D., Pemberton, J.M., Clutton-Brock, T.H., Crawley, M.J., 1998. Noise and determinism in synchronised sheep dynamics. Nature 394, 673–677.

Gross, T., Ebenhoh, W., Feudel, U., 2006. Long food chains are in general chaotic. OIKOS 109(1), 135–144.

Hastings, A., Powell, T., 1991. Chaos in a three-species food chain. Ecology 72, 896–903.

Hillary, R.M., Bees, M.A., 2004. Plankton lattices and the role of chaos in plankton patchiness. Phys. Rev. E 69(031913).

Lalli, C.M., Parsons, T.R., 1997. Biological Oceanography: An Introduction. Butterworth-Heinemann, Open University.

Levy, M., Klein, P., 2004. Does the low frequency variability of mesoscale dynamics explain a part of the phytoplankton and zooplankton spectral variability? Proc. R. Soc. Lond. A 460, 1673–1687.

Martin, A.P., 2003. Phytoplankton patchiness: The role of lateral stirring and mixing. Prog. Oceanogr. 57, 125–174.

Martin, A.P., Richards, K.J., 2002. Patchy productivity in the open ocean. Global Biogeochem. Cycles 16(2), 1025–1034.

Okubo, A., 1971. Oceanic diffusion diagrams. Deep-Sea Res. 18, 789–802.

Pikovsky, A., Michael, R., Kurths, J., 2001. Synchronisation: A Universal Concept in Nonlinear Sciences. Cambridge University Press, Cambridge, UK.

Popova, E.E., 1995. Non-universal sensitivity of a robust ecosystem model of the ocean upper mixed layer. Ocean Model. 109, 2–5.

Popova, E.E., Lozano, C.J., Srokosz, M.A., Fasham, M.J.R., Haley, P.J., Robinson, A.R., 2002. Coupled 3D physical and biological modelling of the mesoscale variability observed in North-East Atlantic in spring 1997: Biological processes. Deep-Sea Res. I 49, 1741–1768.

Slater, R.D., 1993. Some parametric and structural simulations with a three-dimensional ecosystem model of nitrogen cycling in the North Atlantic euphotic zone. In: Evans, G.T., Fasham, M.J.R. (Eds.), Towards a Model of Ocean Biogeochemical Processes, vol. 10. NATO. Springer-Verlag, Berlin.

Smith, C.L., Richards, K.J., Fasham, M.J.R., 1996. The impact of mesocale eddies on plankton dynamics in the upper ocean. Deep-Sea Res. I 43, 1807–1832.

Srokosz, M.A., Martin, A.P., Fasham, M.J.R., 2003. On the role of biological dynamics in plankton patchiness at the mesoscale: An example from the eastern North Atlantic ocean. J. Mar. Res. 61, 517–537.

Steele, J.H., Henderson, E.W., 1981. A simple plankton model. Am. Nat. 344, 734–741.

Strogatz, S., 1994. Nonlinear Dynamics and Chaos: With Applications to Physics, Biology, Chemistry and Engineering. Westview Press, Perseus Books Group.

Totterdell, I.J., 1993. An annotated bibliography of marine biological models. In: Evans, G.T., Fasham, M.J.R. (Eds.), Towards a Model of Ocean Biogeochemical Processes, vol. 10. NATO. Springer-Verlag, Berlin.